Entangled Images from Four-Wave Mixing
Vincent Boyer, *et al.*
Science **321**, 544 (2008);
DOI: 10.1126/science.1158275

Entangled Images from Four-Wave Mixing

Vincent Boyer,* Alberto M. Marino, Raphael C. Pooser, Paul D. Lett*

Two beams of light can be quantum mechanically entangled through correlations of their phase and intensity fluctuations. For a pair of spatially extended image-carrying light fields, the concept of entanglement can be applied not only to the entire images but also to their smaller details. We used a spatially multimode amplifier based on four-wave mixing in a hot vapor to produce twin images that exhibit localized entanglement. The images can be bright fields that display position-dependent quantum noise reduction in their intensity difference or vacuum twin beams that are strongly entangled when projected onto a large range of different spatial modes. The high degree of spatial entanglement demonstrates that the system is an ideal source for parallel continuous-variable quantum information protocols.

Images have always been a communication medium of choice because of the large amount of information they can carry in their details. Up to the present, optical devices have mostly ignored the phase and intensity fluctuations that result from the quantum nature of the light that transports the images. The ability of modern detectors to see the quantum fluctuations of light has triggered the emergence of the field of quantum imaging, where "visual" information can be contained not only in the local intensity of a light field but also in the local quantum fluctuations (*1*). Controlling these local fluctuations can improve optical resolution (*2*), image amplification (*3*), and beam positioning (*4*). Seen in the context of quantum information science, quantum imaging is an extension of quantum optics to the transverse spatial degrees of freedom, and it allows us to benefit from the intrinsic parallelism of image processing. Here, we demonstrate the production of highly multimode quantum-correlated "twin beams" by nondegenerate four-wave mixing (4WM) in a hot atomic vapor. The beams display continuous-variable (CV) entanglement in that the quantum fluctuations of a given pair of spatial modes cannot be described independently, a property also known as inseparability. This property is needed for the implementation of numerous quantum information protocols (*5*).

CV-entangled light can be generated with a phase-insensitive optical amplifier (*6*), which mixes and amplifies two field modes a and b (the probe and the conjugate), generating twin beams. When fed with coherent states, vacuum states, or both, the amplifier produces a pure state whose entanglement manifests itself through strong correlations between the fluctuations of the output probe and conjugate fields. These fields are each described quantum mechanically by a pair of conjugate quadrature operators: $(\hat{X}_a, \hat{Y}_a)$ for the probe and $(\hat{X}_b, \hat{Y}_b)$ for the conjugate. The variance of these operators for coherent states sets the quantum noise level (QNL) of the quadrature fluctuations. They are normalized here so that the QNL is unity. To describe the correlations between the twin beams, we define the joint quadrature operators $\hat{X}_- = (\hat{X}_a - \hat{X}_b)/\sqrt{2}$ and $\hat{Y}_+ = (\hat{Y}_a + \hat{Y}_b)/\sqrt{2}$, which combine the quadrature operators of the individual fields. For an amplifier gain (*6*) larger than one, the fluctuations $\langle \Delta \hat{X}_-^2 \rangle = \langle \Delta \hat{Y}_+^2 \rangle$ are squeezed: They are smaller than the QNL. The squeezing is larger for a larger amplifier gain. Reciprocally, the observation of noise reduction with respect to the QNL on both joint quadratures $\hat{X}_-$ and $\hat{Y}_+$ for two optical fields is sufficient to prove their entanglement, or inseparability. More generally, the degree of inseparability can by quantified by $I = \langle \Delta \hat{X}_-^2 \rangle + \langle \Delta \hat{Y}_+^2 \rangle$. The states are inseparable when $I < 2$ (*7*, *8*). Inseparability has been demonstrated for single–spatial-mode twin beams, which can be likened to single pixel images, with optical parametric oscillators (OPOs) operating below (*9*, *10*) and above threshold (*11*, *12*), with 4WM in optical fibers (*13*) and with mixing of single-mode squeezed states, giving the best measured inseparability to date of $I = 0.56$ (*14*).

A multi–spatial-mode optical amplifier couples many pairs of spatial modes $\{(a_i, b_i)\}$, so that the quantum fluctuations of the twin beams depend not only on the frequency but also on the spatial variables. Multimode operation occurs naturally in amplifiers using nonlinear processes such as parametric down-conversion (PDC) [$\chi^{(2)}$ nonlinearity] or 4WM [$\chi^{(3)}$ nonlinearity], as long as the phase-matching condition allows a range of probe and conjugate wave vectors to be coupled (*15*). Multi–spatial-mode entanglement has been observed in PDC (*16*, *17*), where the gain is inherently low, via photon-counting and coincidence techniques. This can be done in spite of the weakness of the quadrature entanglement and the low detector efficiency. Here, we produce states with large quadrature entanglement that can be detected efficiently.

Large gains can be obtained with a $\chi^{(2)}$ medium in an OPO configuration, where a build-up cavity enhances the nonlinearity (*18*), but these devices have proved challenging to operate in the multi–spatial-mode regime. A possible remedy is direct synthesis of multimode quantum light (*4*, *19*). Another route, which we present here, is 4WM in atomic vapors, which display very large nonlinearities. The recent demonstration of a large quantum noise reduction in the intensity difference of twin beams generated by nondegenerate 4WM in a hot vapor of ^{85}Rb without the use of a cavity (*20*) has prompted our interest in observing spatial quantum effects in $\chi^{(3)}$ media. The scheme (Fig. 1A) follows a double-lambda configuration (*21*, *22*) in which a strong pump field of frequency ω_0 is mixed (by way of the interaction with four atomic levels) with two weak fields of frequencies ω_a and ω_b (the probe and the conjugate) such that $\omega_a + \omega_b = 2\omega_0$ (*23*). The fundamental feature of the scheme

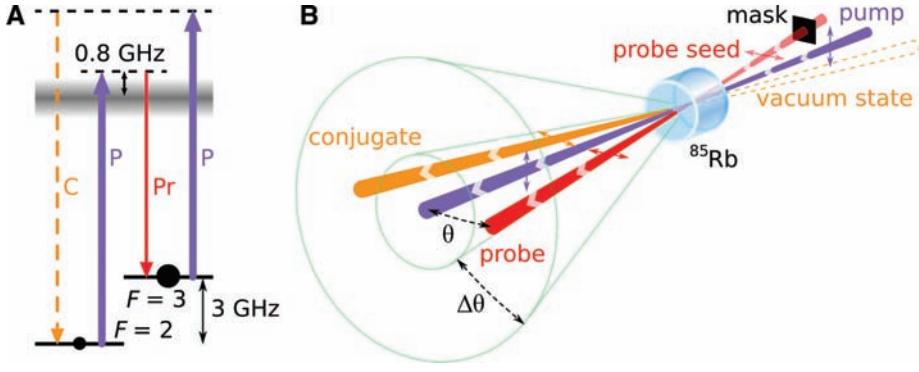

Fig. 1. 4WM in a hot ^{85}Rb vapor. (**A**) Atomic levels of the $D1$ transition of ^{85}Rb involved in the double-lambda scheme. The width of the excited state represents the Doppler broadening. The pump (P) puts most of the atomic population in the $F = 3$ hyperfine electronic ground state. The parametric process converts two pump photons into one probe (Pr) photon and one conjugate (C) photon, which leads to quantum correlations between the fields. (**B**) Geometry of the experiment. The bright pump is focused in a hot ^{85}Rb vapor cell and couples with probe and conjugate fields located symmetrically at a small angle θ with respect to the pump axis. The coupling is substantial over a range of angles $\Delta\theta$ and has a cylindrical symmetry. The coupling region is schematically represented by the green solid angle. When the process is seeded in a particular probe mode, as represented in this figure, this mode and the corresponding conjugate mode (initially in a vacuum state) emerge as bright twin beams. Arbitrarily shaped twin beams can be obtained by inserting an amplitude mask on the probe seed. The polarization of the fields is indicated by the double arrows.

Joint Quantum Institute, National Institute of Standards and Technology, University of Maryland, Gaithersburg, MD 20899, USA.

*To whom correspondence should be addressed. E-mail: vincent.boyer@nist.gov (V.B.); paul.lett@nist.gov (P.D.L.)

is that the light fields are coupled via the coherence between the two hyperfine ground states, with a minimum amount of atomic population in the excited state. This strongly suppresses the spontaneous emission and, along with the large detunings, reduces the absorption of the probe and the conjugate fields. In this condition, and in the limit of low pump depletion, the system behaves like a near-perfect phase-insensitive amplifier for the probe and the conjugate (*24*).

The phase-matching condition dictates that the beams in the 4WM be nearly colinear, with the probe and the conjugate propagating at the same small angle θ with respect to the pump, on either side of it (Fig. 1B). The finite length of the medium slightly relaxes the longitudinal phase-matching condition and allows for a range of angles Δθ, effectively setting the angular acceptance of the process. The angular resolution of the amplifier is the angular size of the smallest optical mode (in the far field) that is coupled to the gain medium. It is diffraction-limited by the transverse size of the gain region, which is controlled by the waist and the intensity of the pump in the vapor. From the angular acceptance and angular resolution, one can estimate that 100 orthogonal pairs of spatial modes are independently coupled in the medium (*23*).

Fig. 2. Intensity-difference squeezing in the multi–spatial-mode regime. An opaque amplitude mask is placed in the far field of the seed, and the high spatial frequencies are filtered out with a pinhole. (**A**) Image of the probe seed in the far field. (**B**) Image of the output probe in the intermediate field. (**C**) Image of the conjugate in the far field. The intensities are normalized to 1. The different optical conjugations for the probe and the conjugate images show the lensing effect due to the cross-Kerr interaction with the pump beam, which acts mostly on the probe. These images demonstrate the optical quality, in the classical sense, of the amplifier. Moreover, intensity-difference measurements on the output probe and the conjugate show that the letters N and T are independently squeezed, which proves the multimode operation of the 4WM.

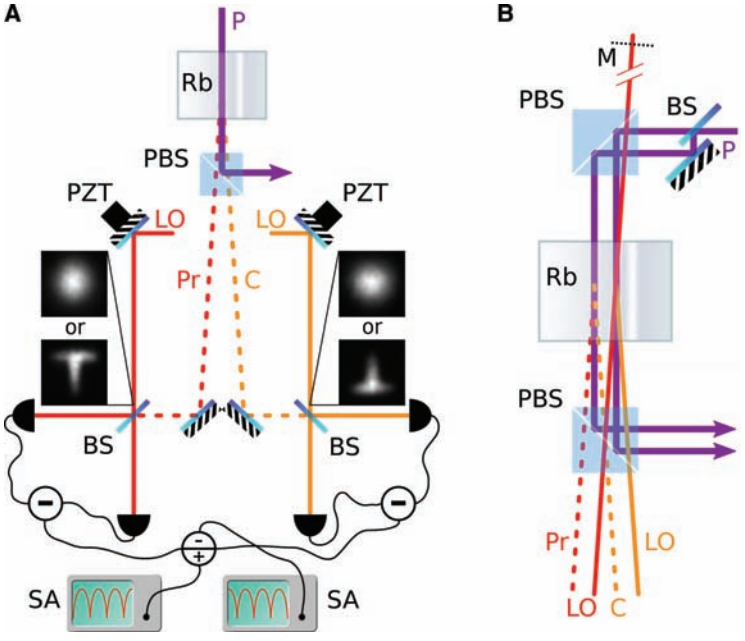

Fig. 3. Entanglement measurement with dual-homodyne detection. The two-mode squeezed vacuum, represented by dashed lines, is nondegenerate and requires two phase-locked LOs with frequencies separated by 6 GHz. (**A**) General layout. P, pump; Pr, probe; C, conjugate; BS, 50/50 beamsplitter; PBS, polarizing beamsplitter; PZT, piezoelectric actuator; Rb, Rubidium vapor cell; SA, spectrum analyzer. A hybrid junction forms the sum and difference of the quadrature signals measured by the HDs, and both the sum and difference noises are recorded simultaneously by two spectrum analyzers. The piezoelectric actuators are scanned synchronously so that the HDs measure the same quadratures at any given time. The images show two possible beam profiles for the LOs. (**B**) Detail of the generation of the LOs. The pump beam is split into two parts of equal power so that the spatial modes of the LOs, created by seeded 4WM, match a pair of entangled spatial modes created by similar unseeded 4WM. In the experiment, the probe, conjugate, and LO beams are not in the same plane, which makes their physical separation easier. An optional amplitude mask (M) placed in the far field of the seed allows for the generation of LOs of arbitrary mode shape.

One way of observing the quantum correlations is to seed the process with a coherent state of intensity I_0 at the probe frequency, whereas the input conjugate is left in a vacuum state (Fig. 1B). The amplification produces bright twin beams of intensities $I_a = GI_0$ for the probe and $I_b = (G-1)I_0$ for the conjugate. The intensity difference $I_a - I_b$ displays a theoretical normalized noise power equal to $1/(2G-1)$, below the QNL of unity. Experimentally, a gain of up to 10 and a quantum noise reduction of more than 8 dB have been observed for Gaussian twin beams (*24*). The multi–spatial-mode operation of the amplifier means that one can produce bright twin beams in any set of spatial modes fitting into the spatial bandwidth of the process and that matching subparts of the twin beams that are contained in the spatial bandwidth should be independently entangled and, in particular, should be intensity-difference squeezed (*25*).

To illustrate this point, we seeded the process with a "NT"-shaped spatial mode created with an opaque amplitude mask, and we recorded the intensity-difference noise power at 3.5 MHz with a balanced detector and a radiofrequency spectrum analyzer. The highest spatial frequencies of the seed, which would not be amplified by the 4WM, were removed with a spatial filter placed before injection in the amplifier. The overall detection efficiency is 90 ± 3% (*26*), and we corrected the measured noise for only the electronic noise floor of the photodetector. Figure 2 shows the input probe, output probe, and output conjugate in the image planes of the mask. Cross-Kerr modulation from the intense pump causes the probe beam to experience a lensing effect as it crosses the pump beam. The same effect is negligible for the conjugate because of the large detuning from the atomic transition. As a result, the image plane of the input mask is located at a different distance for the probe and the conjugate. Apertures select which part of each output beam hits the balanced detector. At a gain $G \approx 4.5$, up to –5.4 ± 0.2 dB of intensity-difference squeezing is recorded for the full NT modes, –5.2 ± 0.2 dB for the "N" subparts, and –5.1 ± 0.2 dB for the "T" subparts, showing that matching subparts of the twin beams are correlated. The smallest size of correlated subparts is determined by the angular resolution, and the intensity difference of unmatched subparts (for instance, the N of one beam and the T of the other beam) displays amplifier excess noise (*25*). The independence of the squeezing of matched local subparts is the hallmark of spatial squeezing (*27*, *28*).

Intensity measurements on bright beams give access to the fluctuations of the amplitude quadratures, which then coincide with the $\hat{X}_a$ and $\hat{X}_b$ quadratures. Alone, they cannot prove entanglement. In fact, one would also expect the phase sum of the fields to be squeezed (*6*, *28*), where the phase quadratures coincide with $\hat{Y}_a$ and $\hat{Y}_b$. Measuring all of the four quadratures $\hat{X}_a$, $\hat{Y}_a$, $\hat{X}_b$, and $\hat{Y}_b$ requires homodyning with local oscilla-

tors (LOs) mode-matched to the pair of modes under interrogation. We tuned the amplifier to have a gain $G \approx 4$, and we fed it with vacuum inputs, so as to generate a two-mode squeezed vacuum output, or vacuum twin beams (dashed lines in Fig. 3A). Two balanced homodyne detectors (HDs) whose phases are scanned synchronously measure the same quadrature on both twin beams at any given time, and the noise of the sum and the difference of the two signals is analyzed at a frequency of 0.5 MHz. The LOs must be phase-locked and separated in frequency by 6 GHz, one at the probe and the other at the conjugate frequency. As the phases are scanned, the HDs successively measure the $\hat{X}$, $\hat{Y}$, $-\hat{X}$, and $-\hat{Y}$ quadratures of both beams for every $\pi/2$ phase shift, and the difference and sum signals alternately measure the $\hat{X}_-$, $\hat{Y}_+$, $-\hat{X}_-$, and $-\hat{Y}_+$ joint quadratures. As shown in Fig. 4A, where Gaussian-shaped LOs were used, the joint quadratures are measured to be squeezed by -4.3 ± 0.2 dB, which fulfills the inseparability criterion $I = 0.74 \pm 0.02 < 2$. Taking into account the finite detection efficiency of 90%, the inferred squeezing would be –5.2 dB, and the inseparability would become $I = 0.60$. There exists a degree of entanglement higher than inseparability—called Einstein-Podolsky-Rosen (EPR) entanglement—that quantifies the possibility of acquiring some knowledge about the quantum nature of the state of one beam by measuring the other one. For twin beams, the conditional variances $V_{X_a|X_b}$ and $V_{Y_a|Y_b}$ are smaller than $2\langle\Delta\hat{X}_-^2\rangle$ and $2\langle\Delta\hat{Y}_+^2\rangle$, respectively (*29*). As a consequence, with our experimental results, $V_{X_a|X_b} \cdot V_{Y_a|Y_b} \leq 4\langle\Delta\hat{X}_-^2\rangle\langle\Delta\hat{Y}_+^2\rangle = 0.55 < 1$, which gives an upper bound for the EPR criteria and is a sufficient condition for the presence of EPR entanglement.

To fulfill the strict criteria of relative-phase stability, we found it convenient to generate the LOs by using the very 4WM process under study, in the spirit of Kim *et al.* (*30*). As explicitly shown in Fig. 3B, the pump beam is equally split into two parts before the vapor cell. One part is used to generate the vacuum twin beams, and the other part is mixed with a probe seed to generate two bright twin beams that we use as LOs. Several points concerning this method deserve discussion. First, all the beams are derived from the same laser and are therefore relative-phase stable. No active phase stabilization is required. Second, the LOs themselves display multi–spatial-mode entanglement, but this has a negligible impact on the measured entanglement of the vacuum twin beams in the limit of well balanced HDs (*23*). Third, the vacuum modes that are analyzed in the HDs are those that completely overlap with the bright part of the LOs. Fourth, the seeded 4WM process produces bright twin beams with slightly unbalanced intensities, resulting in HDs with unequal optical gains. We can correct for this by adjusting the electronic gain of one of the balanced detectors, but at the level of squeezing that we observe and at our operating gain we found that this has little impact. Lastly, the major advantage of the method is that the analyzed spatial modes are automatically matched, because the LOs themselves are generated in a gain medium having the same characteristics as the one used to generate the vacuum twin beams, such as the Kerr-lensing effect. This feature is particularly important when analyzing multi–spatial-mode squeezed light, because any mismatch between the modes selected by the HDs leads to the partial detection of noisy and uncorrelated optical modes. This adds excess noise to the signal and can bring the recorded noise well above the QNL, as has already been observed for intensity-difference squeezing (*25*). This is in contrast to the case where only a single spatial mode experiences gain. In that case, mode mismatch in the HDs merely results in a loss of detection efficiency, which leads only to a reduced level of measured squeezing. The effect of the excess noise in the imperfectly mode-matched HDs might explain why our best measured squeezing occurs at a rather low amplifier gain.

The multi–spatial-mode operation of the amplifier is demonstrated by the arbitrariness of the position and angle of the LOs, which only have to be chosen symmetrically with respect to the pump direction and inside the solid angle of acceptance. This point can be made even more clear by putting a mask on the probe beam seeding the LOs, in this case a T. Both LOs then carry a T image, as shown in Fig. 4B. The noise of the joint quadratures is slightly increased to –3.6 dB, with respect to the QNL, while remaining well below the inseparability and the EPR limits. Figure 4B also shows the transverse profile of the LOs in the detection region and the far field for the conjugate LO, highlighting the differential lensing effect experienced by the probe and the conjugate LOs. Of course, the vacuum twin beams are also subject to the same effect and the mode matching between the vacuum modes interrogated by the two LOs occurs naturally. On the other hand, it would be difficult to construct ad hoc LOs with properly matched transverse profiles.

Quadrature entanglement can therefore be demonstrated using as LOs any pair of bright twin images that can be created by the 4WM process. For instance, the generation of bright Laguerre-Gauss twin beams has already been demonstrated in this system (*25*). Because Laguerre-Gauss modes of first order are a superposition of TEM_{10} and TEM_{01} (transverse electromagnetic) modes, this hints at the fact that entanglement should be observed with LOs in the TEM_{10} and TEM_{01} modes. This, in turn, would imply that Gaussian-shaped bright twin beams created by 4WM are entangled in their position and momentum (*31*). In the general case, the quadrature variables of a pair of spatial modes cannot be interpreted as familiar conjugate variables of a pair of bright beams, such as their positions and momenta, but the entanglement of these quadratures corresponds to the most general form of spatial entanglement (*32*).

The analysis of the multi–spatial-mode vacuum twin beams by means of pairs of bright beams used as LOs also sheds some light on the complexity of the spatial entanglement. Such a set of spatially orthogonal pairs of modes would

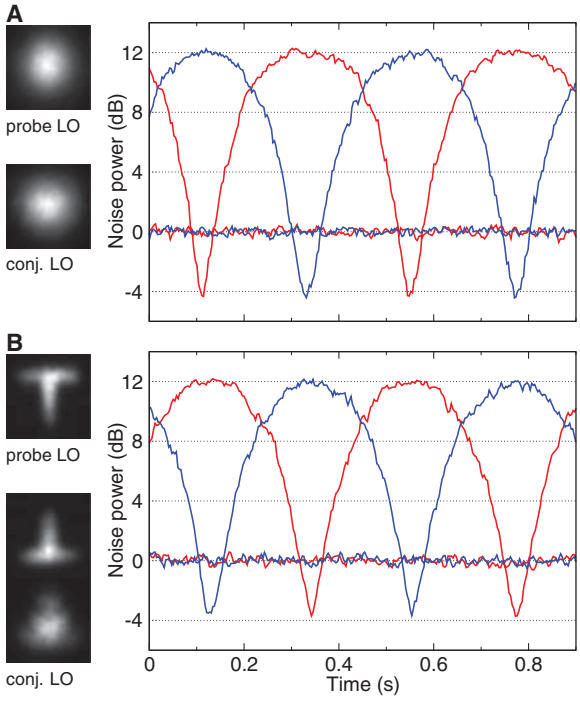

Fig. 4. Quadrature squeezing. The traces show the normalized noise power of the sum (blue) and difference (red) of the quadratures measured by the two HDs, as the phases of the LOs are scanned simultaneously. When the two-mode squeezed vacuum is blocked, the HDs record the QNL, which is set at 0 dB. When the fields emitted by the 4WM are measured, the difference and sum noise curves drop successively below the QNL, revealing the squeezing of both $\hat{X}_-$ and $\hat{Y}_+$. $\langle\Delta\hat{X}_-^2\rangle$ and $\langle\Delta\hat{Y}_+^2\rangle$ correspond to the minima of the red and blue curves, respectively. The images on the left show the intensity profile of the LOs at the position of the HDs. (**A**) Entanglement for Gaussian modes, with –4.3 dB of squeezing on both joint quadratures. (**B**) Entanglement for T-shaped modes. The minimum noise is –3.6 dB for both traces. The conjugate mode is shown both at the position of the HD (lower image) and in the far field (upper image). The LOs appear to have similar spatial modes but not the same focal plane.

correspond to the eigenmodes of the Schmidt decomposition of the biphoton wave function created in the 4WM process. This type of theoretical analysis was carried out for PDC (*33*). A measure of the spatial entanglement is provided by the Schmidt number, which is the "average" number of Schmidt modes involved. A rough estimate of that number is given by the number of gain-medium diffraction-limited Gaussian twin beams that fit into the solid angle of acceptance (*23*), and it naturally matches the previous estimate of the number of independent modes, counted in terms of non-overlapping coherence areas (*25*, *34*). Such a large Schmidt number highlights the potential of this system as a source of high-dimensional entanglement. The exact details of the entanglement, contained in the coefficients of the Schmidt decomposition, depend on the spatial gain profile and can be tuned by varying the spatial mode of the pump laser. A major challenge will be to use that degree of freedom to generate and detect useful multimode states.

References and Notes

1. M. I. Kolobov, Ed., *Quantum Imaging* (Springer, New York, 2007).
2. M. I. Kolobov, C. Fabre, *Phys. Rev. Lett.* **85**, 3789 (2000).
3. A. Mosset, F. Devaux, E. Lantz, *Phys. Rev. Lett.* **94**, 223603 (2005).
4. N. Treps *et al.*, *Science* **301**, 940 (2003).
5. S. L. Braunstein, P. van Loock, *Rev. Mod. Phys.* **77**, 513 (2005).
6. M. D. Reid, P. D. Drummond, *Phys. Rev. Lett.* **60**, 2731 (1988).
7. L.-M. Duan, G. Giedke, J. I. Cirac, P. Zoller, *Phys. Rev. Lett.* **84**, 2722 (2000).
8. R. Simon, *Phys. Rev. Lett.* **84**, 2726 (2000).
9. Z. Y. Ou, S. F. Pereira, H. J. Kimble, K. C. Peng, *Phys. Rev. Lett.* **68**, 3663 (1992).
10. J. Laurat, T. Coudreau, G. Keller, N. Treps, C. Fabre, *Phys. Rev. A* **70**, 042315 (2004).
11. A. S. Villar, L. S. Cruz, K. N. Cassemiro, M. Martinelli, P. Nussenzveig, *Phys. Rev. Lett.* **95**, 243603 (2005).
12. J. Jing, S. Feng, R. Bloomer, O. Pfister, *Phys. Rev. A* **74**, 041804 (2006).
13. C. Silberhorn *et al.*, *Phys. Rev. Lett.* **86**, 4267 (2001).
14. H. Yonezawa, S. L. Braunstein, A. Furusawa, *Phys. Rev. Lett.* **99**, 110503 (2007).
15. P. Kumar, M. I. Kolobov, *Opt. Commun.* **104**, 374 (1994).
16. A. Mair, A. Vaziri, G. Weihs, A. Zeilinger, *Nature* **412**, 313 (2001).
17. J. C. Howell, R. S. Bennink, S. J. Bentley, R. W. Boyd, *Phys. Rev. Lett.* **92**, 210403 (2004).
18. L. Lopez, N. Treps, B. Chalopin, C. Fabre, A. Maître, *Phys. Rev. Lett.* **100**, 013604 (2008).
19. M. Lassen *et al.*, *Phys. Rev. Lett.* **98**, 083602 (2007).
20. C. F. McCormick, V. Boyer, E. Arimondo, P. D. Lett, *Opt. Lett.* **32**, 178 (2007).
21. P. R. Hemmer *et al.*, *Opt. Lett.* **20**, 982 (1995).
22. M. D. Lukin, P. R. Hemmer, M. O. Scully, *Adv. At. Mol. Opt. Phys.* **42**, 347 (2000).
23. Materials and methods are available as supporting material on *Science* Online.
24. C. F. McCormick, A. M. Marino, V. Boyer, P. D. Lett, preprint available at http://arxiv.org/abs/quant-ph/0703111 (2007).
25. V. Boyer, A. M. Marino, P. D. Lett, *Phys. Rev. Lett.* **100**, 143601 (2008).
26. All uncertainties quoted in this paper represent 1 SD, combined statistical and systematic uncertainties.
27. M. I. Kolobov, *Rev. Mod. Phys.* **71**, 1539 (1999).
28. P. Navez, E. Brambilla, A. Gatti, L. A. Lugiato, *Phys. Rev. A* **65**, 013813 (2001).
29. M. D. Reid, *Phys. Rev. A* **40**, 913 (1989).
30. C. Kim, P. Kumar, *Phys. Rev. Lett.* **73**, 1605 (1994).
31. V. Delaubert *et al.*, *Phys. Rev. A* **74**, 053823 (2006).
32. M. T. L. Hsu, W. P. Bowen, N. Treps, P. K. Lam, *Phys. Rev. A* **72**, 013802 (2005).
33. C. K. Law, J. H. Eberly, *Phys. Rev. Lett.* **92**, 127903 (2004).
34. O. Jedrkiewicz *et al.*, *Phys. Rev. Lett.* **93**, 243601 (2004).

35. R.C.P. is supported under a grant from the Intelligence Community Postdoctoral Program.

Supporting Online Material

www.sciencemag.org/cgi/content/full/1158275/DC1
Materials and Methods
SOM Text
Figs. S1 and S2
References

25 March 2008; accepted 4 June 2008
Published online 12 June 2008;
10.1126/science.1158275
Include this information when citing this paper.

Phase Transitions of Dirac Electrons in Bismuth

Lu Li,[1]* J. G. Checkelsky,[1] Y. S. Hor,[2] C. Uher,[3] A. F. Hebard,[4] R. J. Cava,[2] N. P. Ong[1]*

The Dirac Hamiltonian, which successfully describes relativistic fermions, applies equally well to electrons in solids with linear energy dispersion, for example, in bismuth and graphene. A characteristic of these materials is that a magnetic field less than 10 tesla suffices to force the Dirac electrons into the lowest Landau level, with resultant strong enhancement of the Coulomb interaction energy. Moreover, the Dirac electrons usually come with multiple flavors or valley degeneracy. These ingredients favor transitions to a collective state with novel quantum properties in large field. By using torque magnetometry, we have investigated the magnetization of bismuth to fields of 31 tesla. We report the observation of sharp field-induced phase transitions into a state with striking magnetic anisotropy, consistent with the breaking of the threefold valley degeneracy.

The Dirac Hamiltonian, long the accepted theory of relativistic fermions, is equally successful in describing electrons in solids, notably bismuth (*1*–*3*), $Bi_{1-x}Sb_x$ (*4*), and graphene (*5*, *6*). Unlike in regular solids, the electron energy, $E(\mathbf{p})$, in these materials is linear in the momentum, $\mathbf{p}$, just as in relativistic fermions. However, Dirac electrons living in solids have two distinguishing features. First, because of their small (or zero) mass gap, the Dirac bands become quantized into Landau levels in a modest magnetic field, $\mathbf{H}$. A striking consequence in graphene is the observation of the integer quantum Hall effect (QHE) (*5*, *6*). The Coulomb interaction energy is crucially important when all electrons are confined to the lowest Landau level. Secondly, the Dirac electrons in solids come in different "flavors," corresponding to orbital valley degeneracy. The interplay of strong interaction and degeneracy suggests that, in intense $\mathbf{H}$, a phase transition may occur to a collective state with novel quantum properties (*7*). In bismuth, the Dirac electrons occupy three Fermi surface (FS) ellipsoids. By using a torque cantilever to measure its magnetization, we have observed sharp field-induced transitions. The high-field ordered state is magnetically anisotropic, consistent with the breaking of the flavor (valley) degeneracy.

In bismuth, the hole FS ellipsoid is aligned with the trigonal axis $\mathbf{z}$ (*8*) (Fig. 1A, inset). The three-electron FS ellipsoids, arrayed symmetrically around the hole FS, are tilted by a small angle β (~6.5°) out of the plane defined by the bisectrix ($\mathbf{x}$) and binary ($\mathbf{y}$) axes. Extensive studies have established that the electron ellipsoids have a Dirac dispersion (*1*, *2*, *9*, *10*). In the geometry with $\mathbf{H}\|\mathbf{z}$, each Landau level of the electrons has a threefold valley degeneracy. However, the near-equality of the hole and electron FS areas (projected onto the *xy* plane) has long stymied efforts to resolve the quantum oscillations of the electrons from the holes (*11*–*14*). This roadblock has to be overcome before the Dirac electrons can be investigated. We solved this problem with torque magnetometry (*8*) [section I of supporting online material (SOM)]. Two sets of data were taken to maximum H =14 T and to 31 T (at temperatures of 1.5 and 0.3 mK, respectively) on single crystals in which the resistance ratio (between 300 K and 4 K) RRR is ~100.

In an increasing $\mathbf{H}$, the Landau level energies rise. As each sublevel crosses the chemical potential μ and empties, a break-in-

[1]Department of Physics, Princeton University, NJ 08544, USA. [2]Department of Chemistry, Princeton University, NJ 08544, USA. [3]Department of Physics, University of Michigan, Ann Arbor, MI 48109, USA. [4]Department of Physics, University of Florida, Gainesville, FL 32611, USA.

*To whom correspondence should be addressed. E-mail: luli@princeton.edu (L.L.); npo@princeton.edu (N.P.O.)